ACS APPLIED MATERIALS & INTERFACES

www.acsami.org

Research Article

Ratiometric Antifouling Electrochemical Biosensors Based on Multifunctional Peptides and MXene Loaded with Au Nanoparticles and Methylene Blue

Yan Xu, Xinyan Wang, Caifeng Ding,* and Xiliang Luo*

Cite This: *ACS Appl. Mater. Interfaces* 2021, 13, 20388−20396

Read Online

ACCESS | Metrics & More | Article Recommendations | Supporting Information

ABSTRACT: A universal strategy for the construction of ratiometric antifouling electrochemical biosensors was developed based on multifunctional peptides and 2D nanomaterial MXene loaded with gold nanoparticles (AuNPs) and methylene blue (MB). The nanocomposite of MXene loaded with AuNPs and MB (MXene-Au-MB) exhibited excellent conductivity, where the AuNPs were able to capture biomolecules containing sulfhydryl terminus, and the MB molecules were used to generate electrochemical signal. The MXene-Au-MB was fixed on the electrode surface by Nafion, and the anchored peptide captured the electrochemical signal probe carboxyl-modified ferrocene (Fc) to construct an electrochemical biosensor. The multifunctional peptide containing the anchoring, antifouling, and recognizing sequences endowed the sensing surface not only the assaying function but also the capability to resist nonspecific adsorption from complex samples. In the biosensing system, with the increase in the target concentration, the electrochemical signal of MB remained constant, whereas the electrochemical signal of Fc gradually decreased, and the ratiometric detection strategy greatly improved the accuracy of the biosensor. In the presence of a model target prostate-specific antigen (PSA), the recognizing sequence was recognized and cleaved, and the ratiometric signal of Fc and MB indicated the concentration of PSA accurately and sensitively, with a detection range from 5 pg/mL to 10 ng/mL and a limit of detection of 0.83 pg/mL. Electrochemical biosensors based on the MXene-Au-MB and multifunctional peptides possessed high selectivity, accuracy, and sensitivity even in real complex biological samples because of the excellent antifouling ability of the peptide. More importantly, the assaying of other targets can be easily realized with a similar biosensing strategy by changing the recognition sequence of the multifunctional peptide, and the detection of thrombin (TB) has also been achieved in this work.

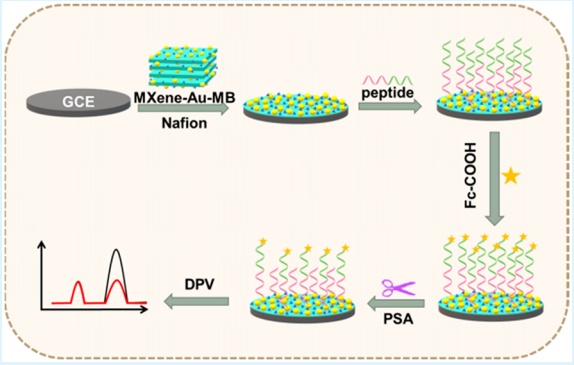

KEYWORDS: *electrochemical biosensor, MXene, antifouling, ratiometric detection, multifunctional peptide*

Downloaded via UNIV OF PRINCE EDWARD ISLAND on May 15, 2021 at 13:08:09 (UTC).
See https://pubs.acs.org/sharingguidelines for options on how to legitimately share published articles.

1. INTRODUCTION

Since they were published for the first time in 2004,[1] two-dimensional (2D) nanomaterials have been widely studied and applied in many fields, such as electrocatalysis, optics, electrochemistry, etc., because of their excellent properties.[2−4] So far, a great quantity of 2D nanomaterials, including boron nano chips (BNSs), black phosphorus (BP), graphite carbon nitride (g-C_3N_4), transition metal oxides (TMOs), and graphene have been discovered.[5−10] Two-dimensional nanomaterials have broad application prospects in electrochemical biosensors because of their large specific surface area and excellent physical and chemical properties.[11] Recently, the new 2D nanomaterial MXene possesses a unique combination of excellent electrical conductivity, easily tunable structure, rich functional groups, hydrophilicity, and large interlayer spacing, making it an attractive research object. In the past few years, MXene has achieved encouraging results in many fields, including energy storage devices,[12−15] photoelectrocatalysis,[16,17] flexible wearable sensors,[18] electronic devices,[19] and photothermal conversion.[20] It should be noted that the unique accordion-like structure, strong reduction ability, and compatibility with other nanomaterials make it easy for MXene to form composites with other materials. It has been proved that MXene has a strong reducing ability and can reduce metal nanoparticles without reducing agents and stabilizers. For example, AuNPs-MXene nanocomposite and MXene/Ag composite have been obtained through the strong reduction ability of MXene and have excellent electrical conductivity and

Received: March 16, 2021
Accepted: April 13, 2021
Published: April 21, 2021

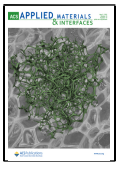

© 2021 American Chemical Society

Scheme 1. Schematic Illustration of Ratiometric Antifouling Electrochemical Biosensor Working Mechanism

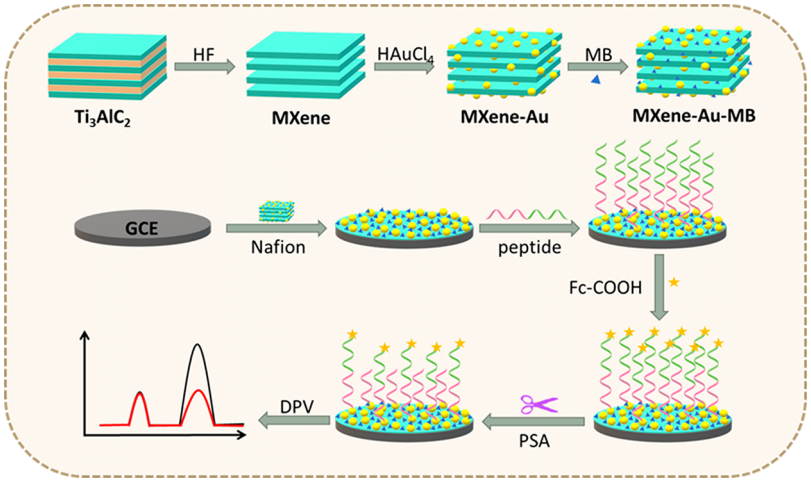

electrocatalytic activity.[21,22] In addition, as an exceptional charge transport accelerator and an excellent immobilization matrix, MXene has considerably high surfaces to volume ratio, exceptional conductivity, and adsorption capacity, which would be quite suitable for electrochemical biosensing, but there is not much research in this area.

As one of the most commonly used detection methods in scientific research, electrochemical biosensors have the advantages of good selectivity, high sensitivity, and simple operation. Nevertheless, it is still a challenge to specifically and accurately detect targets in complex biological samples because of nonspecific adsorption of biomolecules to the sensing interface. So it is urgent to build an antifouling interface to improve the selectivity and lifetime of electrochemical sensing. Currently, the most commonly used antifouling materials are polyethylene glycol (PEG)[23−25] and zwitterionic materials.[26,27] However, PEG is susceptible to oxidative damage when being used for a long time, whereas most zwitterionic materials cannot be synthesized easily. In recent years, Luo's group has been designing and synthesizing series of zwitterionic peptides as antifouling materials because of their excellent biocompatibility, a convenient synthesis process, and design that allows them to be highly hydrophilic and electrically neutral as required.[28−33]

The internal standard method has attracted more and more attention to effectively avoid the potential influence of internal and external factors.[34,35] Our group has constructed a dual-signal ECL cytosensor with high sensitivity and reliability,[36] in which luminol was used as the internal standard molecule, and CdTe quantum dot (QD) was used as the signal molecule to be labeled on the cancer cell aptamer to indicate the number of cancer cells. The ratiometric dual signal spectrum effectively eliminates the interference in the system to get more accurate detection results, even in a complex environment. Previous work has also proved that the built-in correction function in the ratio strategy can minimize the deviation between multiple electrodes and effectively overcome the potential impact of system or background noise.[33,34,37−39]

In the present work, gold nanoparticles (AuNPs) grew on the surface of MXene in situ without additional reductant and stabilizer. Meanwhile, methylene blue (MB), as an electrochemical internal molecule, was also decorated to the MXene-Au to form a novel nanocomposite material (MXene-Au-MB). Subsequently, the nanocomposite material was fixed to the surface of the electrode with the help of Nafion. After modifying with a designed multiple-functional peptide, which has an anchor sequence (CPPPP), an antifouling sequence (DRDRDRD), and a recognizing sequence (HSSKLQK for PSA, GSRPVLG for TB),[33] an antifouling sensing surface with excellent conductivity and large specific surface area was obtained. Aspartic acid (D) and lysine (K) are both hydrophilic amino acids, and D is negatively charged and K is positively charged. So the hydrophilic and electrical neutral antifouling sequence has an antifouling property. By changing the recognizing sequence of the peptide, we can detect prostate-specific antigen (PSA) and thrombin (TB), respectively, indicating a universal ratiometric antifouling electrochemical biosensor was constructed successfully.

EXPERIMENTAL SECTION

Synthesis of Ti_3C_2Tx-MXene. MXene is made by etching Al in Ti_3AlC_2 with HF at room temperature.[40] Briefly, 2 mg of Ti_3AlC_2 powder and 8 mL of 40% HF solution were mixed and stirred for 48 h at room temperature. After the etched reaction, the material was washed repeatedly by deionized water and centrifuged until the supernatant reached a pH ≥6. The precipitate was then dried in vacuum at 60 °C for 12 h to obtain MXene for future use.

Synthesis of MXene-Au. MXene-Au nanocomposite was synthesized according to refs 21 and 22. First, 1 mg of MXene was added to 5 mL of deionized water and sonicated for 20 min to make it evenly dispersed in water. The $HAuCl_4$ (1 mL, 20 mM) solution was then added dropwise under stirring. After 5 min of reaction, the supernatant and precipitate were separated by centrifuging and washing three times. Finally, the precipitate was dried in a vacuum at 60 °C for 12 h to obtain MXene-Au for subsequent use.

Synthesis of MXene-Au-MB. MXene-Au composite was added into a 10 μM MB solution and treated by ultrasonicated for 30 min, the MB molecules were adsorbed on MXene-Au to obtain the MXene-Au-MB nanocomposite through electrostatic adsorption. The excess MB was removed by centrifugation and washing three times.

Construction of the Electrochemical Sensing Surface. A glassy carbon electrode (GCE) was polished and ultrasonically cleaned before use. The MXene-Au-MB solution containing 5% Nafion was fixed on the surface of the GCE electrode and naturally dried at room temperature. The modified electrode was incubated in a 0.2 mg/mL peptide solution (containing 10 mM TCEP) at 4 °C for 12 h and then washed three times with PBS to remove unreacted peptides to obtain the peptide/MXene-Au-MB/GCE sensing interface. Ferrocenedicarboxylic acid (Fc) was dispersed in PBS containing EDC (0.4 M) and NHS (0.1 M) and incubated for 1 h to activate the carboxyl group on the Fc. Subsequently, the peptide/MXene-Au-MB/

https://doi.org/10.1021/acsami.1c04933
ACS Appl. Mater. Interfaces 2021, 13, 20388−20396

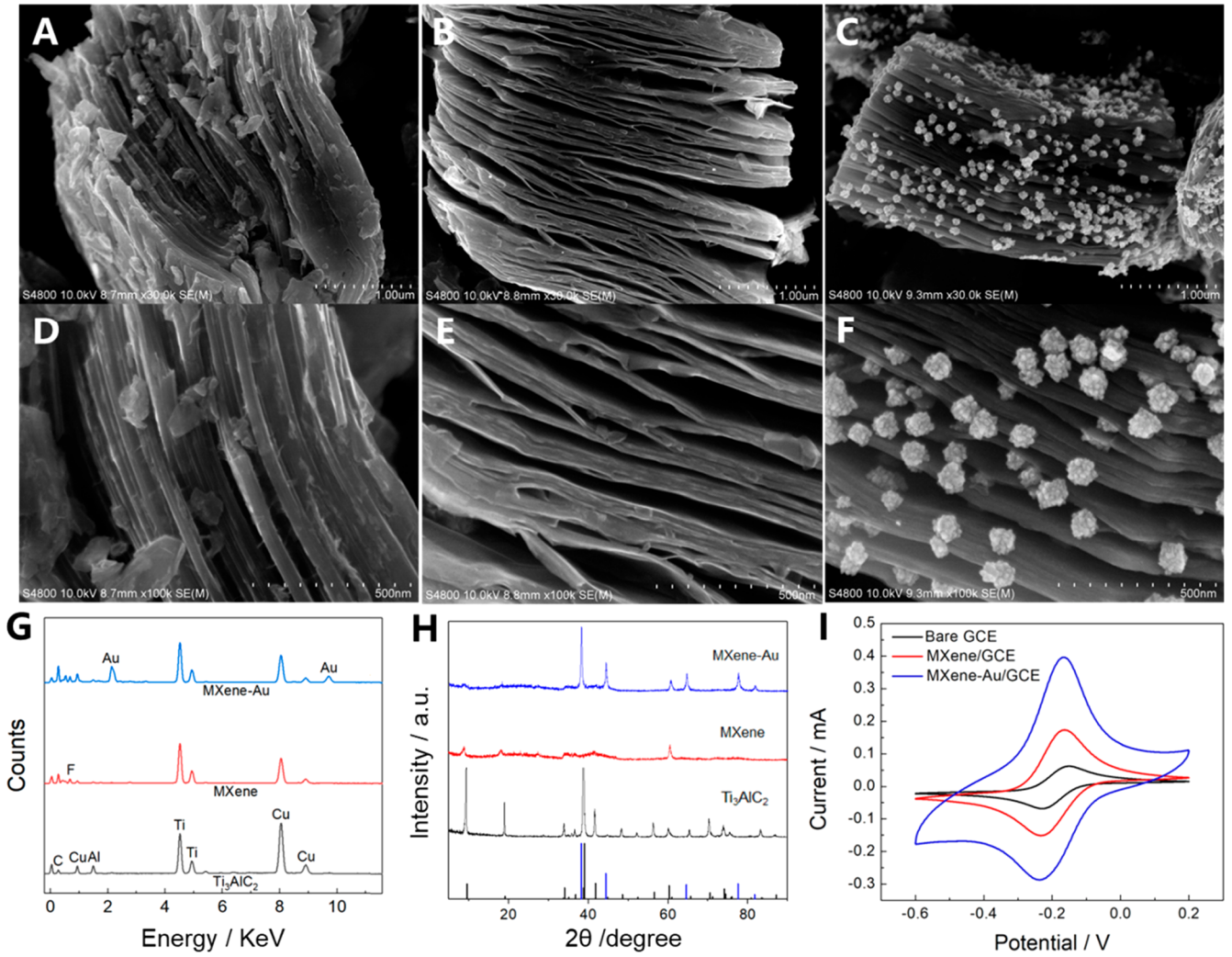

Figure 1. SEM images of (A, D) Ti_3AlC_2, (B, E) MXene, and (C, F) MXene-Au composite at different magnifications. (G) EDS spectra and (H) XRD patterns of Ti_3AlC_2, MXene, and MXene-Au composite. (I) CVs at bare GCE, MXene/GCE, and MXene-Au/GCE in 5 mM $[Ru(NH_3)_6]^{3+}$ containing 0.1 M KCl by scanning the potential from −0.6 to 0.2 V at a scan rate of 0.1 V/s.

GCE electrode was incubated in activated Fc solution for 2 h to construct the Fc/peptide/MXene-Au-MB/GCE sensing interface via amide bonds. Finally, the electrode was washed with PBS buffer three times.

Electrochemical Measurements. The Fc/peptide/MXene-Au-MB/GCE sensing interface was incubated in PSA solution for 40 min. After washing with PBS, the biosensor response data were recorded using DPV, the scanning potential is from −0.5 to 0.5 V, the amplitude is 50 mV, the pulse period is 0.5 s, and the potential increment is 4.0 mV.

RESULTS AND DISCUSSION

Response Mechanism of the Ratiometric Antifouling Electrochemical Biosensor. As shown in Scheme 1, after the Al layer in Ti_3AlC_2 was etched by HF to obtain MXene, AuNPs were synthesized on MXene material to obtain MXene-Au by an in situ synthesis method. MXene is a stable and powerful loading platform for adsorbing organic dyes,[41,42] and the strong electrostatic adsorption (Figure S1) between MXene-Au and MB makes MB firmly loaded into MXene-Au to obtain MXene-Au-MB nanocomposite. After fixing the MXene-Au-MB to the GCE with Nafion, the specific surface area and the conductivity of the electrode is greatly improved. At the same time, MB can be introduced into the electrode surface as an internal standard molecule. In addition, AuNPs can provide peptide binding sites so that the peptides can be immobilized on the electrode surface through Au−S bonds. The other end of the peptide has an amino group, so the Fc can be captured on the modified electrode surface through the amide bond. In the presence of targets, the free part of the peptide can be recognized and cleaved. Fc molecules fall off from the electrode surface, resulting in a decrease in the DPV signal of Fc, whereas the signal of MB remains unchanged. The ratio change of Fc and MB signals can be used to determine the PSA concentration. More importantly, one part of the peptide is designed to have antifouling performance, so the biosensor can detect PSA in human serum and other complex medium with a quite good selectivity. It is worth noting that by changing the recognition sequence in the peptide, the same detection theory can be applied to the highly selective and sensitive detection of other targets.

Characterization of Ti_3AlC_2, MXene, MXene-Au, and MXene-Au-MB. The morphology and elements of MXene, MXene-Au, and MXene-Au-MB are recorded by SEM, EDS, XRD, and fluorescence, and obvious changes can be observed from Figure 1. After the Al element is corroded, Ti_3AlC_2 with a densely stacked layered structure (Figure 1A, D) becomes

https://doi.org/10.1021/acsami.1c04933
ACS Appl. Mater. Interfaces 2021, 13, 20388−20396

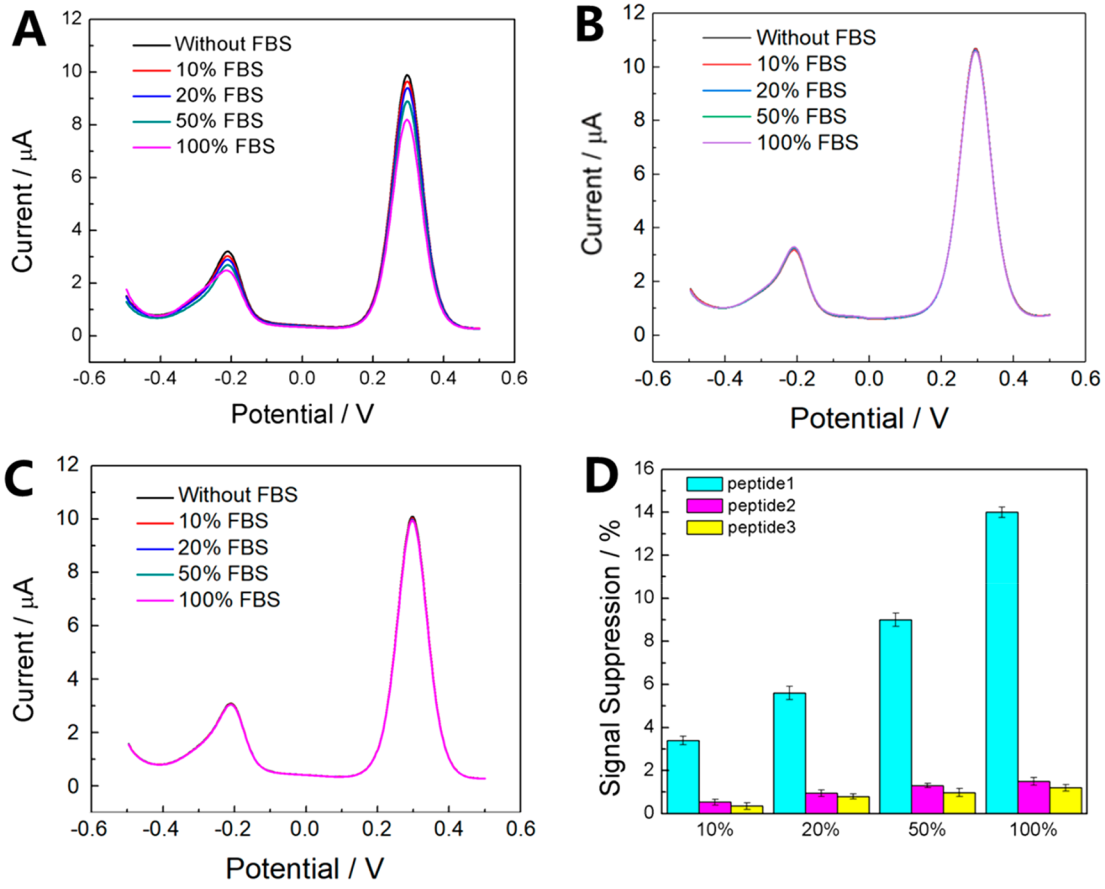

Figure 2. DPV responses in PBS (0.1 M, pH 7.4) of biosensor with (A) peptide1 (general peptide), (B) peptide2 (antifouling peptide) and (C) peptide3 (cleaved antifouling peptide) before and after incubation in FBS samples with different concentrations. (D) Antifouling performance analysis histogram of biosensor with peptide1 (blue), peptide2 (pink), and peptide3 (yellow) based on the signal change of Fc.

MXene with an accordion-like multilayer structure (Figure 1B, E). After in situ synthesis of AuNPs, a large number of AuNPs (Figure 1C, F) with a size of about 50 nm can be seen on the surface of MXene material. The composition of Ti_3AlC_2 before and after HF treatment and the synthesis of MXene-Au are illustrated by EDS. As shown in Figure 1G, Al element that exists in Ti_3AlC_2 (black line) decreases significantly and the F element appears (red line) after HF etching. When AuNPs are in situ synthesized to the surface of MXene, the Au element appears (blue line), demonstrating the successful synthesis of MXene-Au. Meanwhile, the phase transition was recorded in XRD mode as shown in Figure 1H. Interestingly, after etching, the peak intensity of the formed MXene becomes extremely weak, indicating that the crystallinity and configuration deformation are significantly reduced compared to the standard comparison card of Ti_3AlC_2. In addition, the (002) peak moves to the lower angle and becomes wider, which is consistent with the results in the literature.[43] In addition, the MXene-Au-MB nanocomposite was characterized by fluorescence spectroscopy, as shown in Figure S2. MXene-Au is nonfluorescent, whereas 10 μM MB detects a fluorescent signal at the emission wavelength of 675 nm. Different amounts of MXene-Au were added to 1 mL of 10 μM MB solution to fully react and then centrifuged to obtain the supernatant, and the fluorescence intensity of the supernatant was detected. The fluorescence intensity of the supernatant directly reflects the adsorption capacity of MXene-Au to MB. With the increase in the amount of MXene-Au added, the fluorescence intensity of the supernatant gradually decreased, indicating that MB was effectively loaded in the MXene-Au nanomaterials through strong electrostatic interaction, indicating that MXene-Au-MB was successfully prepared.

As shown in Figure 1I, the electrochemical behavior of MXene-Au is characterized by CV. Obviously, modification of MXene increases the redox peak current and the introduction of AuNPs further elevates the redox peak current. This is because both MXene and AuNPs can effectively increase the conductivity of the electrode. The specific surface areas of bare GCE, MXene/GCE, and MXene-Au/GCE are measured using an electrochemical method and shown in Figure S3. The cyclic voltammetry curves of different modified electrode surfaces at different scanning speeds in 5 mM $[Ru(NH_3)_6]^{3+}$ (pH 7.4, 25 °C) were studied. According to the Randles-Sevcik equation, the electrochemical active area is calculated: $I_p = 2.69 \times 10^5 AD^{1/2}cv^{1/2}$. Here, I_p is the peak current (in A), A is the electrochemical active area (in cm^2), D is the diffusion coefficient of 5 mM $[Ru(NH_3)_6]^{3+}$ (6.0×10^{-6} cm^2/s), c is the concentration of $[Ru(NH_3)_6]^{3+}$ (5×10^{-3} M), and v is the scan rate (in V/s). Through calculation, $A_{(bare\ GCE)}$ is 0.06163 cm^2, $A_{(MXene/GCE)}$ is 0.21066 cm^2, and $A_{(MXene\text{-}Au/GCE)}$ is 0.42277 cm^2, the electrochemically active area has a significant increase. The excellent conductivity and large specific surface area are both beneficial to enhance the sensing performance and sensitivity.

Characterization of the Developed Biosensing Interfaces. The construction of the sensing interface and the

https://doi.org/10.1021/acsami.1c04933
ACS Appl. Mater. Interfaces 2021, 13, 20388−20396

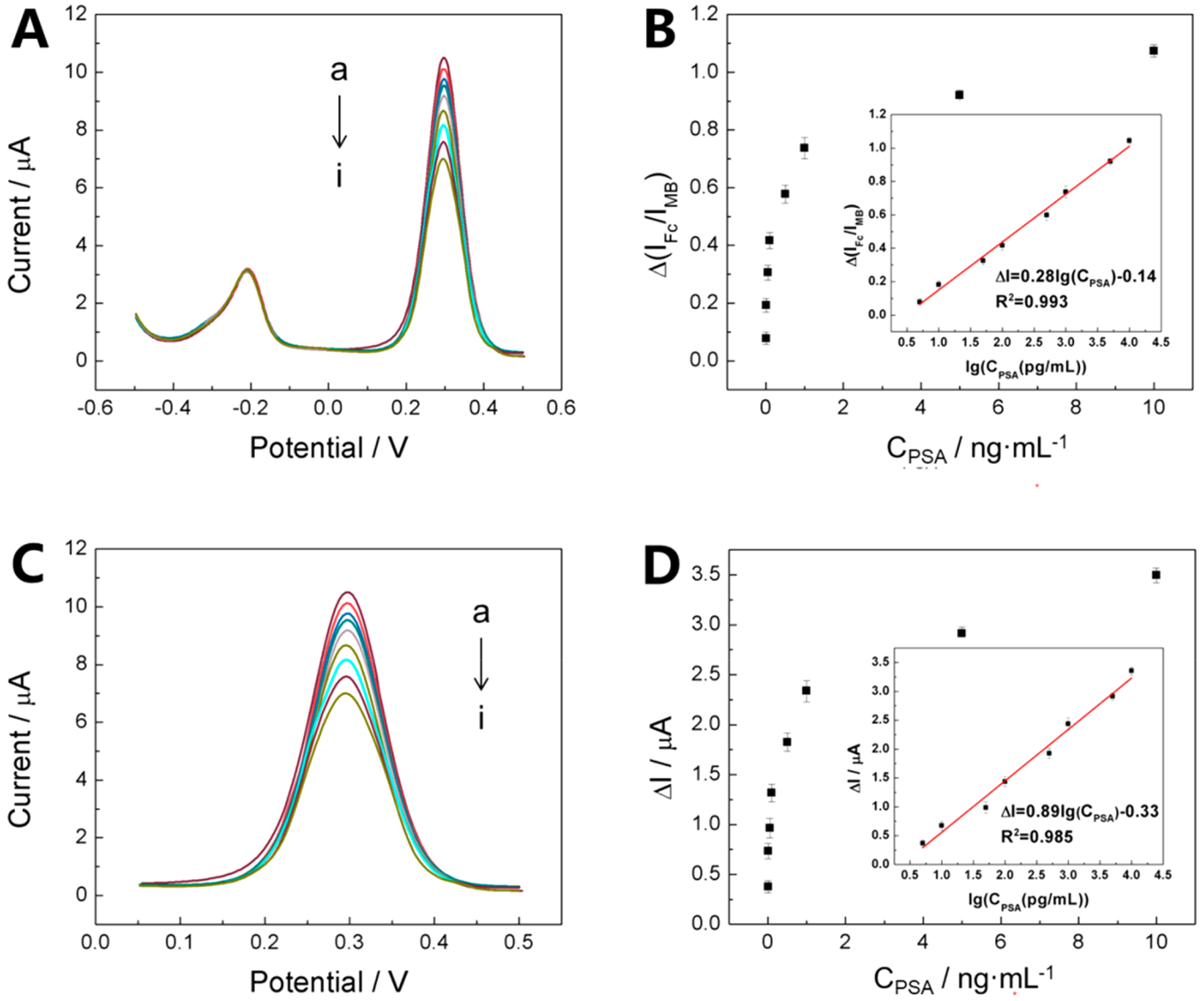

Figure 3. (A) In the presence of an internal standard, the DPV response of the sensing interface under different PSA concentrations: (a) 0 pg/mL, (b) 5 pg/mL, (c) 10 pg/mL, (d) 50 pg/mL, (e) 0.1 ng/mL, (f) 0.5 ng/mL, (g) 1 ng/mL, (h) 5 ng/mL, and (i) 10 ng/mL. (B) PSA calibration curve with internal standard. (C) Sensing interface responds to the DPV signal of PSA without the internal standard. (D) PSA calibration curve without internal standard.

feasibility of the sensor were evaluated by ESI and DPV as shown in Figure S4. The diameter of the semicircle in the impedance spectrum is equal to the electron transfer resistance (R_{et}), which is used to indicate the electron transfer ability of the redox probe at the electrode interface. It can be observed from Figure S4A that the diameter of the semicircle is significantly reduced after the electrode surface is modified with MXene compared to bare GCE. After modifying MXene-Au-MB, the diameter of the semicircle is further reduced. This indicates that MXene and AuNPs can effectively accelerate electron transfer between the redox probe and the electrodes. After modifying the peptide, the impedance increased significantly because of the nonconductivity of the peptide. The conductivity of Fc tagged on the peptide can almost be ignored compared to the nonconductivity of the peptide. From Figure S4B, we can see that the DPV curves of bare GCE (black line) and MXene-Au/GCE (yellow line) have no oxidation peak in PBS solution. After the MXene-Au-MB nanocomposite is fixed on the electrode surface, the oxidation peak of MB can be detected at about −0.2 V (red line). The peptide is then anchored on the electrode surface, Fc is captured, and the oxidation peak of Fc appeared at the position of +0.3 V (blue line), which proves the successful construction of the sensing interface. After incubating the modified electrode in PSA solution for a period of time, it can be found that the DPV signal of Fc was significantly reduced (green line) indicating the releasing of Fc induces by the recognizing and cutting of the peptide sequence by PSA. From the results in Figure S4B, we can see that the DPV signal of MB remains almost unchanged. All of the results prove that the electrochemical biosensors are constructed as expected.

The static water contact angle is used to evaluate and confirm the hydrophilicity and wettability of the electrode surface. From Figure S5 and Table S1, we can see that the MXene-Au-MB has good hydrophilicity because of its large number of hydroxyl groups. Compared to bare GCE, the water contact angle of MXene-Au-MB/GCE is reduced from 57.29 to 28.98°. When the peptide and Fc are immobilized on the

https://doi.org/10.1021/acsami.1c04933
ACS Appl. Mater. Interfaces 2021, 13, 20388−20396

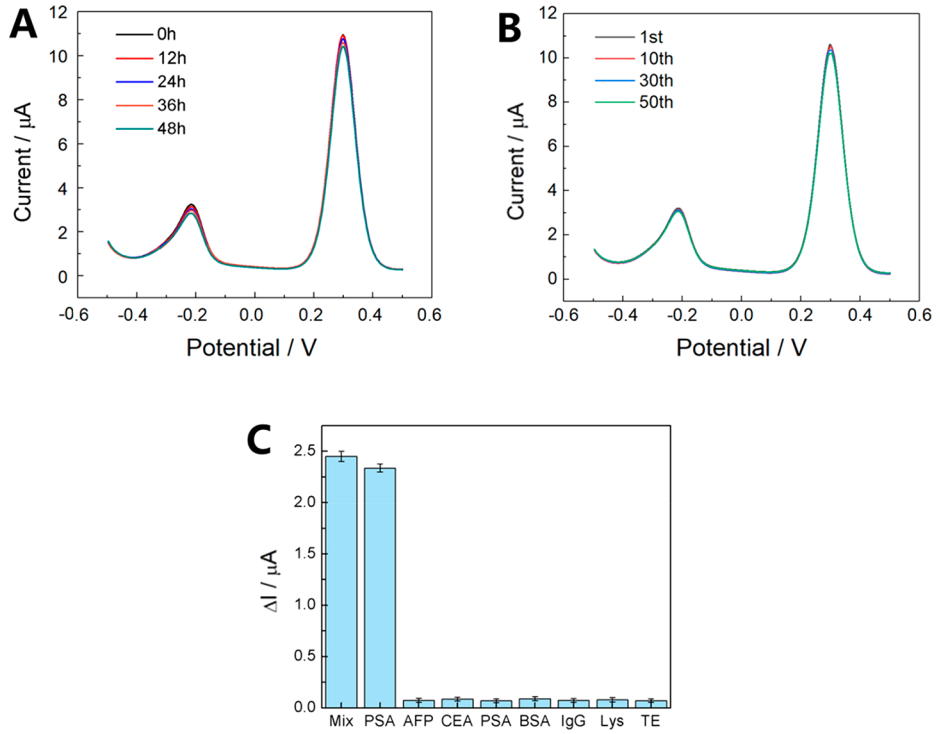

Figure 4. (A) DPV responses of biosensor after immersing in PBS (0.1 M, pH 7.4) for 0, 12 24, 36, and 48 h. (B) DPV responses of the biosensor after 1, 10, 30, and 50 consecutive scans in PBS (0.1 M, pH 7.4). (C) Selectivity of the biosensor for PSA.

electrode surface, the water contact angle is further reduced to 21.07° because of the excellent hydrophilicity of the peptide (in fact, peptide1, 2, 3 are hydrophilic, with almost no difference in contact angle). Excellent hydrophilic interface is one of the important factors for the antifouling of the sensor.

In addition to excellent hydrophilicity, electrical neutrality is another important factor for antifouling biosensors. The zeta potential of the peptide in Figure S6 showed that the designed peptide shows good electrical neutrality before (peptide2) and after (peptide3) cutting.

Generic Antifouling Characteristics. To evaluate the antifouling ability of the sensing surface, we used three kinds of peptides to modify the electrode. One is the general peptide (peptide1), one is the antifouling peptide (peptide2), and one is the cleaved antifouling peptide (peptide3). Different electrode surfaces were incubated in fetal bovine serum (FBS) for 30 min, and the nonspecific adsorption capacity of different interfaces was compared by DPV method as shown in Figure 2A–C. By analyzing the changes of the Fc signal, it can be seen from Figure 2D that after incubation in 100% FBS, the DPV signal of biosensor with general peptide modification decreased by 14.06%, because peptide1 is positively charged (Figure S6A) and contains hydrophobic amino acids (L, H), it may adsorb proteins. And the DPV signal of biosensor with antifouling peptide modification decreased by 1.55% and the DPV signal of biosensor with cleaved antifouling peptide modification also only decreased by 1.2%. These results are the perfect evidence of the antifouling performance of the biosensor due to the good resistance to nonspecific adsorption of the antifouling peptide.

Electrochemical Detection of PSA and TB with Constructed Biosensor. It can be observed from Figure 3A that the Fc DPV signal is significantly reduced with increasing PSA concentration, whereas the MB signal changes slightly. This result is consistent with expectation of the internal standard method. The biosensor has a wider detection range and a lower detection line (Table S3). As shown in Figure 3A, B, a correlation coefficient of 0.993 is shown in the detection range of 5 pg/mL to 10 ng/mL. The corresponding regression equation is $\Delta I = 0.28\lg(C_{PSA}) - 0.14$ and the corresponding detection limit is calculated as 0.83 pg/mL. When there is no internal standard signal molecule, the measured correlation coefficient is 0.985, and the corresponding detection limit is 1.52 pg/mL, which is worse than the biosensor with internal standard signal molecule (Figure 3C, D). From the results, we can see that the measurement accuracy can be improved by the internal standard method. More importantly, by changing the recognition sequence of the peptide, the biosensor also achieves a highly selective and accurate detection of TB. The detection range is 0.1 pM to 10 nM, the detection line is 16.1 fM, and the linear correlation coefficient is 0.995 (Figure S7A, B), which are better than other detection methods (Table S4). In addition, when there is no internal standard, the detection limit of the biosensor for TB is 42.5 fM, and the linear correlation coefficient is 0.981, which is worse than the result when there is an internal standard (Figure S7C, D).

Selectivity and Stability of the Biosensor. The stability of the biosensor is tested using the DPV method. After immersing in PBS buffer for 48 h, the signal still remained 95% of the initial value (Figure 4A). As shown in Figure 4B, after DPV scans 50 times continuously, the DPV signal almost remains unchanged. Bovine serum albumin (BSA), alpha fetoprotein (AFP), thrombin (TB), carcinoembryonic antigen (CEA), and immunoglobulin G (IgG) are used as possible interferences to evaluate the selectivity of the electrochemical biosensor. Under the same conditions, 10.0 ng/mL BSA, AFP, TB, CEA, IgG, Lys, and TE, 1.0 ng/mL PSA and all mixtures

https://doi.org/10.1021/acsami.1c04933
ACS Appl. Mater. Interfaces 2021, 13, 20388−20396

were incubated with the biosensor, respectively. As shown in Figure 4C, the DPV signal (ΔI) increases greatly only when PSA exists ($\Delta I = I_0 - I_1$, I_0 is the current value of Fc before reaction and I_1 is the current value of Fc after reaction). With the same results, the excellent selectivity of the biosensor for TB detection is shown in Figure S8. All of the above proves that the biosensor has excellent stability, internal reproducibility, and selectivity.

Clinical Serum Sample Analysis. The biosensor was used to analyze and detect PSA clinical serum samples provided by the Affiliated Hospital of Heze Medical College. The accuracy of the biosensor for PSA detection in actual samples was compared with or without internal standards. It can be seen from Table 1 that the relative error of the internal standard

Table 1. Analytical Results of PSA in Clinical Serum Samples

sample	ECL method (ng/mL)	this method (ng/mL)	relative error (%)	RSD (%)	method without internal standard (ng/mL)	relative error (%)
1	1.57	1.52	−3.2	3.9	1.43	−8.9
2	5.31	5.18	−2.4	2.1	4.96	−6.6
3	8.23	8.56	4.0	2.4	7.51	−8.7

method (<4.0%) is far less than that without the internal standard method (<8.9%), which indicates that the internal standard method can improve the measurement accuracy. The results are consistent with the data provided by the conventional ECL method in the Affiliated Hospital of Heze Medical College, which shows that its clinical application is feasible. By adding the standard recovery method, the biosensor is also suitable for detecting TB in human serum samples with relative error less than 3.5% (Table S2).

CONCLUSIONS

A novel nanocomposite of MXene loaded with Au nanoparticles and methylene blue was successfully prepared and used for the construction of ratiometric antifouling electrochemical biosensors together with multifunctional peptides. The MXene-Au-MB possesses excellent electrochemical activity, and the Au nanoparticles can be used for biomolecules immobilization, whereas the MB can be used as an internal standard to generate reference electrochemical signal, which greatly improves the reproducibility of the sensor and the accuracy of detection. In addition, the designed multifunctional peptides exhibit excellent antifouling capability, which can allow the biosensor to detect targets in complex biological samples with low fouling. More importantly, the biosensing system has been proved to be a universal antifouling detection strategy by changing the recognition sequence of the peptides. The MXene-Au-MB combined with various functional peptides can be used for the construction of different ratiometric antifouling electrochemical biosensors with high sensitivity and accuracy even in complex biological media.

ASSOCIATED CONTENT

Supporting Information

The Supporting Information is available free of charge at https://pubs.acs.org/doi/10.1021/acsami.1c04933.

Materials and instruments, zeta potential, fluorescence spectrum, characterization of specific surface area, ESI and DPV characterization, static water contact angle, and electrochemical detection of TB (PDF)

AUTHOR INFORMATION

Corresponding Authors

Caifeng Ding − *Key Laboratory of Optic-electric Sensing and Analytical Chemistry for Life Science, Ministry of Education, Shandong Key Laboratory of Biochemical Analysis, Key Laboratory of Analytical Chemistry for Life Science in Universities of Shandong, College of Chemistry and Molecular Engineering, Qingdao University of Science and Technology, Qingdao 266042, PR China*; orcid.org/0000-0002-5281-0158; Phone: +86-532-84022700; Email: dingcaifeng@qust.edu.cn; Fax: +86-532-84022681

Xiliang Luo − *Key Laboratory of Optic-electric Sensing and Analytical Chemistry for Life Science, Ministry of Education, Shandong Key Laboratory of Biochemical Analysis, Key Laboratory of Analytical Chemistry for Life Science in Universities of Shandong, College of Chemistry and Molecular Engineering, Qingdao University of Science and Technology, Qingdao 266042, PR China*; Email: xiliangluo@qust.edu.cn

Authors

Yan Xu − *Key Laboratory of Optic-electric Sensing and Analytical Chemistry for Life Science, Ministry of Education, Shandong Key Laboratory of Biochemical Analysis, Key Laboratory of Analytical Chemistry for Life Science in Universities of Shandong, College of Chemistry and Molecular Engineering, Qingdao University of Science and Technology, Qingdao 266042, PR China*

Xinyan Wang − *Key Laboratory of Optic-electric Sensing and Analytical Chemistry for Life Science, Ministry of Education, Shandong Key Laboratory of Biochemical Analysis, Key Laboratory of Analytical Chemistry for Life Science in Universities of Shandong, College of Chemistry and Molecular Engineering, Qingdao University of Science and Technology, Qingdao 266042, PR China*

Complete contact information is available at: https://pubs.acs.org/10.1021/acsami.1c04933

Notes

The authors declare no competing financial interest.

ACKNOWLEDGMENTS

We acknowledge the financial support of the National Natural Science Foundation of China (22074074, 21974075), the Natural Science Foundation of Shandong Province (ZR2019BB055), the Taishan Scholar Program of Shandong Province of China (Grant ts20110829), and the Qingdao Science and Technology Demonstration Guidance Project (20-3-4-53 nsh).

REFERENCES

(1) Novoselov, K. S.; Geim, A. K.; Morozov, S. V.; Jiang, D.; Zhang, Y.; Dubonos, S. V.; Grigorieva, I. V.; Firsov, A. A. Electric Field Effect in Atomically Thin Carbon Films. *Science* **2004**, *306* (5696), 666.

(2) Allen, M. J.; Tung, V. C.; Kaner, R. B. Honeycomb Carbon: A Review of Graphene. *Chem. Rev.* **2010**, *110* (1), 132−145.

(3) Wang, H.; Maiyalagan, T.; Wang, X. Review on Recent Progress in Nitrogen-Doped Graphene: Synthesis, Characterization, and Its Potential Applications. *ACS Catal.* **2012**, *2* (5), 781−794.

(4) Shao, Y.; Wang, J.; Wu, H.; Liu, J.; Aksay, I. A.; Lin, Y. Graphene Based Electrochemical Sensors and Biosensors: A Review. *Electroanalysis* **2010**, *22* (10), 1027−1036.
(5) Zhang, X.; Xie, Y. Recent Advances in Free-standing Two-Dimensional Crystals with Atomic Thickness: Design, Assembly and Transfer Strategies. *Chem. Soc. Rev.* **2013**, *42* (21), 8187−8199.
(6) Zhuang, X.; Mai, Y.; Wu, D.; Zhang, F.; Feng, X. Two-Dimensional Soft Nanomaterials: A Fascinating World of Materials. *Adv. Mater.* **2015**, *27* (3), 403−427.
(7) Kalantar-Zadeh, K.; Ou, J. Z.; Daeneke, T.; Mitchell, A.; Sasaki, T.; Fuhrer, M. S. Two Dimensional and Layered Transition Metal Oxides. *Applied Materials Today* **2016**, *5*, 73−89.
(8) Liu, H.; Du, Y.; Deng, Y.; Ye, P. D. Semiconducting Black Phosphorus: Synthesis, Transport Properties and Electronic Applications. *Chem. Soc. Rev.* **2015**, *44* (9), 2732−2743.
(9) Zhang, J.; Chen, Y.; Wang, X. Two-Dimensional Covalent Carbon Nitride Nanosheets: Synthesis, Functionalization, and Applications. *Energy Environ. Sci.* **2015**, *8* (11), 3092−3108.
(10) Ji, X.; Kong, N.; Wang, J.; Li, W.; Xiao, Y.; Gan, S. T.; Zhang, Y.; Li, Y.; Song, X.; Xiong, Q.; Shi, S.; Li, Z.; Tao, W.; Zhang, H.; Mei, L.; Shi, J. A Novel Top-Down Synthesis of Ultrathin 2D Boron Nanosheets for Multimodal Imaging-Guided Cancer Therapy. *Adv. Mater.* **2018**, *30* (36), 1803031.
(11) Chimene, D.; Alge, D. L.; Gaharwar, A. K. Two-Dimensional Nanomaterials for Biomedical Applications: Emerging Trends and Future Prospects. *Adv. Mater.* **2015**, *27* (45), 7261−7284.
(12) Zhang, Y.; Mu, Z.; Lai, J.; Chao, Y.; Yang, Y.; Zhou, P.; Li, Y.; Yang, W.; Xia, Z.; Guo, S. MXene/Si@SiOx@C Layer-by-Layer Superstructure with Autoadjustable Function for Superior Stable Lithium Storage. *ACS Nano* **2019**, *13* (2), 2167−2175.
(13) Liang, X.; Garsuch, A.; Nazar, L. F. Sulfur Cathodes Based on Conductive MXene Nanosheets for High-Performance Lithium-Sulfur Batteries. *Angew. Chem., Int. Ed.* **2015**, *54* (13), 3907−3911.
(14) Xie, Y.; Naguib, M.; Mochalin, V. N.; Barsoum, M. W.; Gogotsi, Y.; Yu, X.; Nam, K.-W.; Yang, X.-Q.; Kolesnikov, A. I.; Kent, P. R. C. Role of Surface Structure on Li-Ion Energy Storage Capacity of Two-Dimensional Transition-Metal Carbides. *J. Am. Chem. Soc.* **2014**, *136* (17), 6385−6394.
(15) Yan, J.; Ren, C. E.; Maleski, K.; Hatter, C. B.; Anasori, B.; Urbankowski, P.; Sarycheva, A.; Gogotsi, Y. Flexible MXene/Graphene Films for Ultrafast Supercapacitors with Outstanding Volumetric Capacitance. *Adv. Funct. Mater.* **2017**, *27* (30), 1701264.
(16) Cheng, Y.; Zhang, Y.; Li, Y.; Dai, J.; Song, Y. Hierarchical Ni_2P/Cr_2CT_x (MXene) Composites with Oxidized Surface Groups as Efficient Bifunctional Electrocatalysts for Overall Water Splitting. *J. Mater. Chem. A* **2019**, *7* (15), 9324−9334.
(17) Guo, Z.; Zhou, J.; Zhu, L.; Sun, Z. MXene: A Promising Photocatalyst for Water Splitting. *J. Mater. Chem. A* **2016**, *4* (29), 11446−11452.
(18) Liao, H.; Guo, X.; Wan, P.; Yu, G. Conductive MXene Nanocomposite Organohydrogel for Flexible, Healable, Low-Temperature Tolerant Strain Sensors. *Adv. Funct. Mater.* **2019**, *29* (39), 1904507.
(19) Lyu, B.; Kim, M.; Jing, H.; Kang, J.; Qian, C.; Lee, S.; Cho, J. H. Large-Area MXene Electrode Array for Flexible Electronics. *ACS Nano* **2019**, *13* (10), 11392−11400.
(20) Li, R.; Zhang, L.; Shi, L.; Wang, P. MXene Ti3C2: An Effective 2D Light-to-Heat Conversion Material. *ACS Nano* **2017**, *11* (4), 3752−3759.
(21) Zhang, H.; Wang, Z.; Wang, F.; Zhang, Y.; Wang, H.; Liu, Y. In Situ Formation of Gold Nanoparticles Decorated Ti_3C_2 MXenes Nanoprobe for Highly Sensitive Electrogenerated Chemiluminescence Detection of Exosomes and Their Surface Proteins. *Anal. Chem.* **2020**, *92* (7), 5546−5553.
(22) Zou, G.; Zhang, Z.; Guo, J.; Liu, B.; Zhang, Q.; Fernandez, C.; Peng, Q. Synthesis of MXene/Ag Composites for Extraordinary Long Cycle Lifetime Lithium Storage at High Rates. *ACS Appl. Mater. Interfaces* **2016**, *8* (34), 22280−22286.
(23) Luo, X.; Xu, Q.; James, T.; Davis, J. J. Redox and Label-Free Array Detection of Protein Markers in Human Serum. *Anal. Chem.* **2014**, *86* (11), 5553−5558.
(24) del Pino, P.; Yang, F.; Pelaz, B.; Zhang, Q.; Kantner, K.; Hartmann, R.; Martinez de Baroja, N.; Gallego, M.; Möller, M.; Manshian, B. B.; Soenen, S. J.; Riedel, R.; Hampp, N.; Parak, W. J. Basic Physicochemical Properties of Polyethylene Glycol Coated Gold Nanoparticles that Determine Their Interaction with Cells. *Angew. Chem., Int. Ed.* **2016**, *55* (18), 5483−5487.
(25) Knop, K.; Hoogenboom, R.; Fischer, D.; Schubert, U. S. Poly(ethylene glycol) in Drug Delivery: Pros and Cons as Well as Potential Alternatives. *Angew. Chem., Int. Ed.* **2010**, *49* (36), 6288−6308.
(26) Luo, X.; Xu, M.; Freeman, C.; James, T.; Davis, J. J. Ultrasensitive Label Free Electrical Detection of Insulin in Neat Blood Serum. *Anal. Chem.* **2013**, *85* (8), 4129−4134.
(27) Mi, L.; Jiang, S. Integrated Antimicrobial and Nonfouling Zwitterionic Polymers. *Angew. Chem., Int. Ed.* **2014**, *53* (7), 1746−1754.
(28) Cui, M.; Wang, Y.; Jiao, M.; Jayachandran, S.; Wu, Y.; Fan, X.; Luo, X. Mixed Self-Assembled Aptamer and Newly Designed Zwitterionic Peptide as Antifouling Biosensing Interface for Electrochemical Detection of Alpha-Fetoprotein. *ACS Sensors* **2017**, *2* (4), 490−494.
(29) Liu, N.; Hui, N.; Davis, J. J.; Luo, X. Low Fouling Protein Detection in Complex Biological Media Supported by a Designed Multifunctional Peptide. *ACS Sensors* **2018**, *3* (6), 1210−1216.
(30) Liu, N.; Song, J.; Lu, Y.; Davis, J. J.; Gao, F.; Luo, X. Electrochemical Aptasensor for Ultralow Fouling Cancer Cell Quantification in Complex Biological Media Based on Designed Branched Peptides. *Anal. Chem.* **2019**, *91* (13), 8334−8340.
(31) Nowinski, A. K.; Sun, F.; White, A. D.; Keefe, A. J.; Jiang, S. Sequence, Structure, and Function of Peptide Self-Assembled Monolayers. *J. Am. Chem. Soc.* **2012**, *134* (13), 6000−6005.
(32) Wang, G.; Han, R.; Su, X.; Li, Y.; Xu, G.; Luo, X. Zwitterionic Peptide Anchored to Conducting Polymer PEDOT for the Development of Antifouling and Ultrasensitive Electrochemical DNA Sensor. *Biosens. Bioelectron.* **2017**, *92*, 396−401.
(33) Ding, C.; Wang, X.; Luo, X. Dual-Mode Electrochemical Assay of Prostate-Specific Antigen Based on Antifouling Peptides Functionalized with Electrochemical Probes and Internal References. *Anal. Chem.* **2019**, *91* (24), 15846−15852.
(34) Li, Y.; Wang, L.; Ding, C.; Luo, X. Highly Selective Ratiometric Electrogenerated Chemiluminescence Assay of DNA Methyltransferase Activity via Polyaniline and Anti-fouling Peptide Modified Electrode. *Biosens. Bioelectron.* **2019**, *142*, 111553.
(35) Lin, Y.; Jia, J.; Yang, R.; Chen, D.; Wang, J.; Luo, F.; Guo, L.; Qiu, B.; Lin, Z. Ratiometric Immunosensor for GP73 Detection Based on the Ratios of Electrochemiluminescence and Electrochemical Signal Using DNA Tetrahedral Nanostructure as the Carrier of Stable Reference Signal. *Anal. Chem.* **2019**, *91* (5), 3717−3724.
(36) Ding, C.; Li, Y.; Wang, L.; Luo, X. Ratiometric Electrogenerated Chemiluminescence Cytosensor Based on Conducting Polymer Hydrogel Loaded with Internal Standard Molecules. *Anal. Chem.* **2019**, *91* (1), 983−989.
(37) Xu, Y.; Wang, Z.; Ding, C.; Luo, X. Ratiometric Antifouling Electrochemiluminescence Biosensor Based on Bi-functional Peptides and Low Toxic Quantum Dots. *Sens. Actuators, B* **2020**, *322*, 128613.
(38) Hao, Q.; Wang, L.; Niu, S.; Ding, C.; Luo, X. Ratiometric Electrogenerated Chemiluminescence Sensor Based on A Designed Anti-fouling Peptide for the Detection of Carcinoembryonic Antigen. *Anal. Chim. Acta* **2020**, *1136*, 134−140.
(39) Shao, K.; Wang, B.; Nie, A.; Ye, S.; Ma, J.; Li, Z.; Lv, Z.; Han, H. Target-Triggered Signal-On Ratiometric Electrochemiluminescence Sensing of PSA Based on MOF/Au/G-Quadruplex. *Biosens. Bioelectron.* **2018**, *118*, 160−166.
(40) Alhabeb, M.; Maleski, K.; Anasori, B.; Lelyukh, P.; Clark, L.; Sin, S.; Gogotsi, Y. Guidelines for Synthesis and Processing of Two-

https://doi.org/10.1021/acsami.1c04933
ACS Appl. Mater. Interfaces 2021, 13, 20388−20396

Dimensional Titanium Carbide ($Ti_3C_2T_x$ MXene). *Chem. Mater.* **2017**, *29* (18), 7633−7644.
(41) Zhang, Y.; Wang, L.; Zhang, N.; Zhou, Z. Adsorptive Environmental Applications of MXene Nanomaterials: A Review. *RSC Adv.* **2018**, *8* (36), 19895−19905.
(42) Zhang, R.; Liu, J.; Li, Y. MXene with Great Adsorption Ability toward Organic Dye: An Excellent Material for Constructing a Ratiometric Electrochemical Sensing Platform. *ACS Sensors* **2019**, *4* (8), 2058−2064.
(43) Ding, L.; Wei, Y.; Li, L.; Zhang, T.; Wang, H.; Xue, J.; Ding, L.-X.; Wang, S.; Caro, J.; Gogotsi, Y. MXene Molecular Sieving Membranes for Highly Efficient Gas Separation. *Nat. Commun.* **2018**, *9* (1), 155.

https://doi.org/10.1021/acsami.1c04933
ACS Appl. Mater. Interfaces 2021, 13, 20388−20396